Arctic Maritime Cyclone Distribution and Trends in the ERA5 Reanalysis

ZIHAN CHEN[a] AND AMANDA H. LYNCH[a,b]

[a] *Institute at Brown for Environment and Society, Brown University, Providence, Rhode Island*
[b] *Department of Earth, Environmental, and Planetary Sciences, Brown University, Providence, Rhode Island*

(Manuscript received 5 February 2021, in final form 20 November 2021)

ABSTRACT: We present a tracking algorithm for synoptic to meso-α-scale Arctic cyclones that differentiates between cold- and warm-core systems. The algorithm is applied to the ERA5 reanalysis north of 60°N from 1950 to 2019. In this dataset, over one-half of the cyclones that meet minimum intensity and duration thresholds can be classified as cold-core systems. Systems that undergo transition, typically from cold to warm core, make up 27.2% of cyclones and are longer lived. The relatively infrequent warm-core cyclones are more intense and are most common in winter. The Arctic-wide occurrence of maritime cyclones has increased from 1979 to 2019 when compared with the period from 1950 to 1978, but the trends have high interannual variability. This shift has ramifications for transportation, fisheries, and extractive industries, as well as impacts on communities across the Arctic.

KEYWORDS: Arctic; Extratropical cyclones; Polar lows

1. Introduction

Arctic cyclones span scales from synoptic to mesoscale, and form in both marine and terrestrial environments, associated with the polar front and with regions of high near surface baroclinicity (Serreze et al. 2001). Perhaps the most impactful of these systems are the maritime polar lows—intense, mesoscale cyclones occurring primarily during winter and spring (October–May), typically poleward of the polar front. Polar lows are often associated with rapid intensification, fast propagation (8–13 m s^{-1}), strong winds (often greater than 25 m s^{-1}), high waves, and heavy precipitation as snow or hail (Rasmussen and Turner 2003). Despite advances in numerical weather prediction, significant challenges remain in understanding Arctic cyclonic developments particularly at these smaller scales (Noer et al. 2011; McInnes et al. 2011). As commercial and industrial development in the Arctic continues to increase (Petrov et al. 2016), intense Arctic cyclones have the potential to exacerbate risks to coastal communities, maritime activities, and economically significant industries in high latitudes.

The European Centre for Medium-Range Weather Forecasts (ECMWF) ERA5 reanalysis (Hersbach et al. 2020) provides promise to address the challenge of capturing Arctic cyclone behavior down to the mesoscales over decadal time scales. As a successor to the ECMWF interim reanalysis (ERA-Interim; Dee et al. 2011), the products derived from the ERA5 reanalysis include significant improvements in horizontal, vertical, and temporal resolution, along with better representations of processes likely to affect mesocyclone developments, such as convection (e.g., Hoffmann et al. 2018). The ERA5 reanalysis also includes temporally consistent sea surface temperature and sea ice cover inputs (Hennermann and Berrisford 2018). As a result, this dataset presents an opportunity to comprehensively track meso-α-scale and a proportion of meso-β-scale cyclonic developments together with synoptic systems in the Arctic maritime environment, and with these, gain a more inclusive picture of the spectrum of these cyclones and their evolution over time.

A spectrum is typically used to characterize the maritime Arctic cyclogenesis arising from baroclinic and convective mechanisms (Emanuel and Rotunno 1989; Nordeng and Rasmussen 1992; Rasmussen and Turner 2003). Synoptic storms and polar lows as baroclinic instabilities are well characterized in several observational case studies (e.g., Nordeng and Rasmussen 1992; Douglas et al. 1995; Claud et al. 2004; Brümmer et al. 2009; Bracegirdle and Gray 2009; Føre et al. 2011, 2012). Mesoscale polar lows as convective systems are conceptualized to develop from thermal instabilities (i.e., in cold air outbreaks, Terpstra et al. 2021); intensification of the vortex and organized circulation is then facilitated by processes such as conditional instability of the second kind, assuming a reservoir for convective available potential energy (Rasmussen 1979) or wind-induced surface heat exchange (Emanuel and Rotunno 1989). Recently, Terpstra et al. (2015) demonstrated that polar low disturbances in an Arctic moist-baroclinic environment can amplify without "an upper-level perturbation, surface fluxes, friction, or radiation": these polar lows have a distinct dependence on atmospheric moist diabatic processes during both the initial development and intensification phases. Haualand and Spengler (2020) later confirmed Terpstra et al.'s (2015) hypothesis and suggested that latent heating, not surface sensible heat fluxes, serves as the dominant diabatic source for the development of polar lows. They argued that the detrimental effect of the surface sensible heat fluxes on cyclone growth can be overcome by the latent heat release associated with moisture input from the latent heat fluxes. Other studies have also highlighted the "hybrid" systems, where a variety of diabatic mechanisms act in concert with adiabatic baroclinic instability (Sardie and Warner 1983; Yanase

Supplemental information related to this paper is available at the Journals Online website: https://doi.org/10.1175/JAMC-D-21-0016.s1.

Corresponding author: Zihan Chen, zihan_chen@alumni.brown.edu

DOI: 10.1175/JAMC-D-21-0016.1

and Niino 2005; Bracegirdle and Gray 2009). For example, Deveson et al. (2002) defined a "Type C" cyclogenesis when an upper-level trough intensifies existing organized convection, and diabatic processes then contribute to intensification in successive phases of the life cycle. The relative importance of these mechanisms and the timing of their contribution vary by case and environmental conditions. In summary, many studies have assessed synoptic and polar lows through detailed observational studies (Joly et al. 1997; Parsons et al. 2017), model simulations (e.g., Lynch et al. 2003; Terpstra et al. 2015), satellite analyses using visible, infrared, and synthetic aperture radar imagery (e.g., Blechschmidt 2008; Noer et al. 2011; Smirnova et al. 2015) and climatologies based on operational analyses (e.g., Zahn and Von Storch 2008; Yanase et al. 2016; Stoll et al. 2018). It is still challenging, however, to systematically characterize the full spectrum of cyclones from meso to synoptic scales from a climatological perspective.

Because of the observational challenge that mesoscale systems present in particular, a more systematic understanding of how representative each of these mechanisms may be has been elusive to date. For their small scale, most polar low climatologies have been derived from radar and satellite data with a primary focus on the Norwegian and Barents Seas (e.g., Bracegirdle and Gray 2008; Zahn and Von Storch 2008; Noer et al. 2011; Smirnova et al. 2015; Rojo et al. 2019). With the recent advances in global atmospheric reanalyses, objective climatologies for larger-scale polar lows and synoptic-scale cyclones have been derived from global gridded datasets such as the ERA-Interim reanalysis. For example, Zappa et al. (2014), Michel et al. (2018), Stoll et al. (2018) and Vessey et al. (2020) all used objective criteria and automated tracking algorithms to identify polar lows within global reanalyses. Michel et al. (2018) tracked polar mesoscale cyclones in the ERA-Interim reanalysis, and they found no significant trend in the cyclone occurrences in the Nordic seas. However, some concerned that the resolution of the reanalysis products might impact on the detection of the mesoscale systems. Smirnova and Golubkin (2017) showed that the Arctic System Reanalysis, version 1 (ASRv1), which had a higher spatial and temporal resolution than the ERA-Interim reanalysis, could significantly improve the representations of rapidly evolving systems particularly at the mesoscale.

This paper offers new insights into the climatology of Arctic synoptic and mesocyclones by presenting objective tracking results based on the ERA5 reanalysis for 1950–2019. The long-term coverage and consistency of ERA5 allows us to systematically investigate the changing frequency, life span, and centers of action of Arctic storms over time. To do this, we used the objective cyclone-tracking algorithm developed by Murakami et al. (2015) and Harris et al. (2016) to track cyclone centers based on mean sea level pressure and to differentiate between warm-core and cold-core systems. Because of the complexity of Arctic cyclonic development, a classification method is also introduced to categorize cyclones with major transitions between cold- and warm-core structures during their lifetimes.

2. Data and methods

a. Climate reanalysis data

We used the ERA5 atmospheric reanalysis to track cyclones north of 60°N. Although some studies have used the ERA-Interim reanalysis to develop cyclone climatology in the Arctic (e.g., Stoll et al. 2018; Vessey et al. 2020), it is likely that ERA-Interim underrepresents polar low frequency and intensity, particularly in comparison with the higher-resolution ASRv1 (Bromwich et al. 2016). ERA5 closes the gap by having a similar grid resolution to ASRv1 (~30 km) and has additional advantages of a long temporal record and 4D-Var data assimilation.

Mean sea level pressure (MSLP), 850-hPa relative vorticity, 700-hPa temperature, and near-surface wind speed (10 m) were the primary fields needed for analysis and were obtained as hourly data. As with other studies that apply objective tracking algorithms, it is important to note that the selection of tracking parameters is somewhat subjective. For example, the tracking of warm-core structures is sensitive to the level of the temperature field selected, as well as other thermal parameters (see the online supplemental material for details). Given the typically shallow structure of cyclones in high-latitude regions, the 700-hPa-level temperature was chosen to represent the thermal structure for the midtroposphere. Other parameter choice consequences and sensitivities are described in sections 2b and 2c below.

At the time that this paper was initially submitted, the ERA5 reanalysis spanned 1979 to the present day. At the time of revision, ECMWF had preliminarily released the extension of ERA5 reanalysis back to 1950. The back-extended ERA5 reanalysis (1950–78), which assimilated mostly conventional observations and a small amount of early satellite data, shows improving quality over time and joins seamlessly with the 1979–present reanalysis data (Bell et al. 2021). Despite some known issues with tropical cyclones and surface temperature in Australia, Bell et al. (2021) demonstrated the fidelity of the back-extended reanalysis with an accurate representation of the North Sea Storm of 1953. To investigate the long-term variation of Arctic cyclones activity, the cyclone-tracking algorithm covered the entire time span of 1950–2019. However, out of caution, the tracking algorithm was run separately for the two periods before and after 1979 for the possibility of remaining inconsistencies in the preliminary release of the ERA5 back extension.

b. Tracking algorithm

Objective cyclone-tracking algorithms are critical tools to understand the context in which cyclone development and propagation takes place, but one must note the variation of tracking results from different algorithms (Neu et al. 2013). High-latitude storms have been tracked by both MSLP-based schemes (e.g., Serreze and Barrett 2008; Zahn et al. 2018) and vorticity-based schemes (e.g., Vessey et al. 2020; Stoll et al. 2021). In this study, we used Harris et al.'s (2016) cyclone-tracking algorithm to detect closed contours in the MSLP field. This approach is similar to the method in Wernli and

TABLE 1. List of tunable parameters used in the cyclone-tracking algorithm of Harris et al. (2016).

Parameter	Long name	Unit	Value used in this study
max_cyrad	Max distance between MSLP minima and the closed pressure contour	km	500
dist_threshold	Max distance allowed between storm centers identified at successive time steps (to be combined into a cyclone track)	km	125
ncontours	No. of closed contours to mark a cyclone system	—	1
cint_slp	MSLP contour interval	hPa	0.5
r_offset_warm	Max distance between temperature max and MSLP min	km	500
dt_crit_warm	Temperature contour interval	K	0.5
r_crit_warm	Radius threshold for searching closed temperature contours	km	500
vort_thresh	Min cyclonic (hemisphere dependent) vorticity needed in a cyclone region to identify a cyclone center	s^{-1}	0.5×10^{-5}
maxSLPthreshold	Max admissible central MSLP	hPa	1021

Schwierz (2006). The strength of the MSLP tracking algorithm used here is its capability of identifying warm-core structures associated with a storm center based on the midtropospheric temperature field. This feature also allows for several tunable parameters that include the system size, the minimum intensity, and the implied tilt (Table 1). The algorithm performs the search following the steps below:

1) Smooth the MSLP field with a second-order filter and search for a local MSLP minimum (no more than 1021 hPa). Then, identify a closed contour 0.5 hPa greater than the MSLP minimum. The flood-fill algorithm recursively finds all the adjacent longitude/latitude grid points with a pressure less than the contour value. If a closed contour is found, the MSLP minimum is labeled as the cyclone center at that time.
2) If a cyclone center is found, search for closed contours that mark the total storm region. Given our interest in tracking cyclones with a horizontal scale of less than 1000 km in diameter (encompassing synoptic and meso-α scales), the threshold of the MSLP contour radius is set to 500 km. To prevent different systems from overlapping, the algorithm runs in parallel for all MSLP minima to search for their respective contours. The maximum 10-m wind speed and 850-hPa vorticity for each storm system are recorded at each time step. To omit weak and insignificant developments, a minimum vorticity threshold is set to be $0.5 \times 10^{-5}\ s^{-1}$.
3) Check if the system has a warm core using the flood-fill approach as above. Fit the 700-hPa temperature with a biquadratic and find the local maximum. The algorithm tries to fit the temperature maximum with a 0.5-K contour. The temperature maximum needs to be within 500 km from the low center, and the temperature contour must also have a radius smaller than 500 km. If such a warm core is found, flag the system with a positive warm-core signal at that time step.
4) At the next time step, identify a low center within a 125-km radius to form a storm track. If multiple low centers are found, only pick the one with the lowest MSLP. This separates a strong system from nearby weak vortices. Repeat the warm-core identification and update the values for maximum wind speed and vorticity for the system. Keep searching at the successive time steps until no cyclone center can be found as a part of the storm track.

Three additional tracking criteria are imposed on the cyclone system: 1) maximum surface wind speed larger than 15 m s^{-1} during its lifetime, 2) total lifetime exceeds 24 h, and 3) maritime cyclogenesis. The last criterion is evaluated by applying the ERA5 land–sea mask to the initial development stage of a system. Each longitude/latitude grid point has a value of 0–1 to represent land–sea ratio, with 0 representing a total ocean coverage of the grid box. The average land–sea ratio of the first 6 h of a detected cyclone track must be smaller than 0.5. Because of the exclusion of terrestrial systems, the common issue with MSLP extrapolation over high orography was thus avoided. Terrestrial developments along the polar front are certainly significant, but the focus in this study is on maritime systems with a view to future analyses of the role of ocean surface baroclinicity. Nevertheless, the parameters selected allow for a highly inclusive and hence representative climatology in the maritime domain.

c. *Cyclone classification*

The algorithm defines warm core as a temperature maximum aloft associated with a pressure minimum (cyclone center). Three thermal parameters are used to adjust the sensitivity of warm-core detection: 1) the interval of temperature contours; 2) distance between MSLP minimum and temperature maximum, which accounts for system tilt; and 3) radius of temperature contour. Among the three parameters, the value of contour interval has a relatively large impact on the number of warm cores detected by the algorithm. Our sensitivity tests show that a larger contours interval is associated with a smaller number of warm cores detected, while increasing the search distance and contour radius allows the algorithm to find more warm cores but increases the risk of spurious associations.

Based on the hourly series of warm-core signals during a storm's lifetime, each system is classified into one of the three types: cold-core, mix-core, or warm-core system. The classification is conducted in the postprocessing step, where the series of warm-core signal is grouped into episodes of consistent signal series lasting 12 h or longer. Depending on the value of a warm-

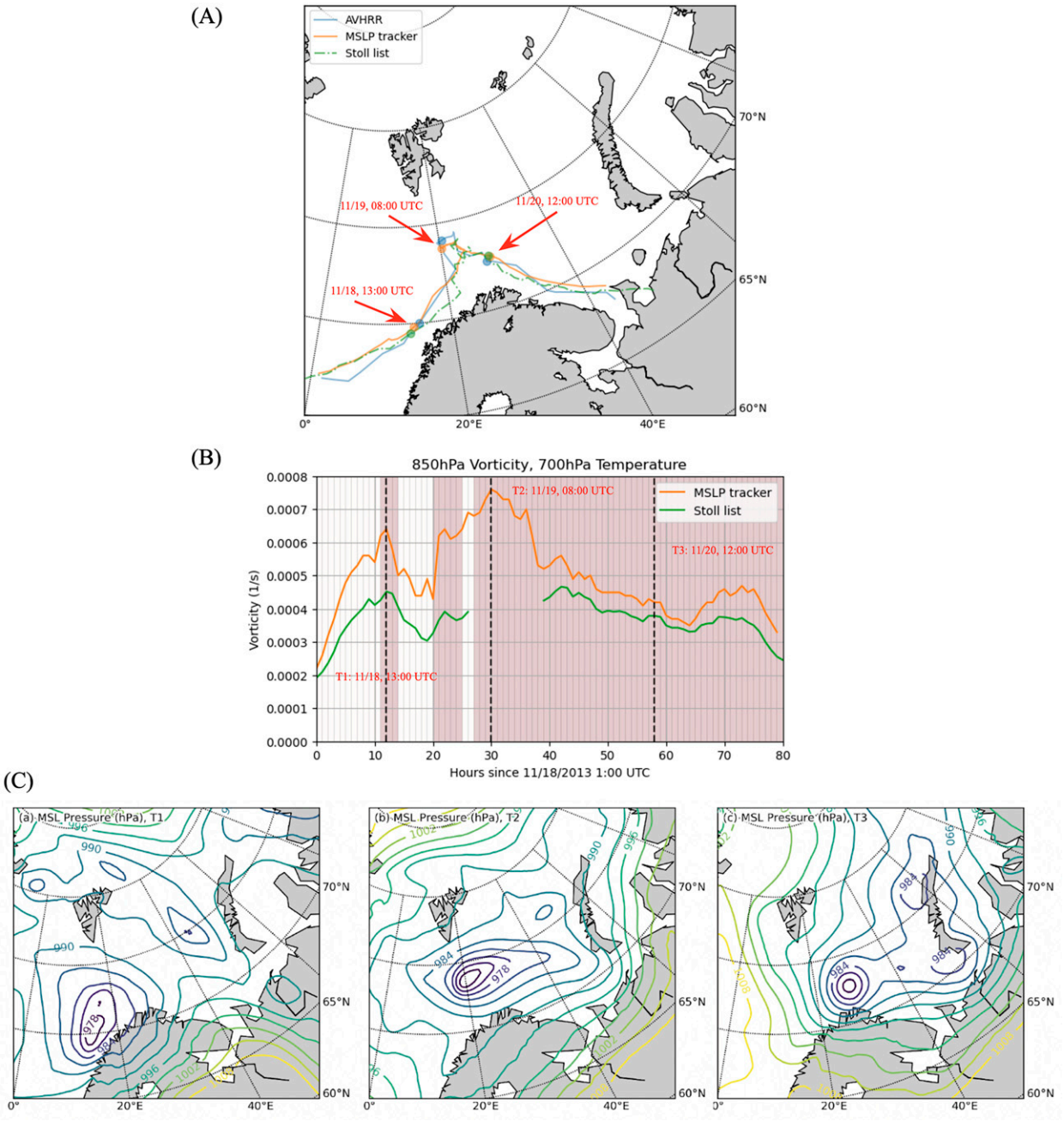

FIG. 1. Case study: (a) Comparison between the algorithm-detected storm track (orange), the one derived from AVHRR satellite imagery (blue), and the same track in the Stoll list (green). (b) The time series of 850-hPa vorticity at the center of the identified cyclone, shaded where a warm-core signal is detected at the 700-hPa level. (c) MSLP contours (hPa) at 1300 UTC 18 Nov 112013, 0800 UTC 19 Nov 2013, and 1200 UTC 20 Nov 2013, indicated by the labels T1, T2, and T3 on the vorticity time series plot.

core signal, each episode is labeled as a warm-core episode (positive signal) or cold-core episode (negative signal). The 12-h time window is selected to ensure the warm-core attribute is stable. Once episodes of consistent cold/warm signals are documented, a warm-core-type system is defined as having only one warm-core episode during its lifetime. Similarly, a cold-core system has only one cold-core episode of consistent negative warm-core flags. The remainder of the cyclones, which exhibit a combination of warm- and cold-core episodes, or an absence of any consistent episode, are classified as the mix-core type. Any sporadic signals that cannot be grouped into a 12-h episode, are ignored. For example, a few cold-core hours could be part of a system classified as warm core as long as they do not form a consistent episode of 12 h or more (see the case study as an example).

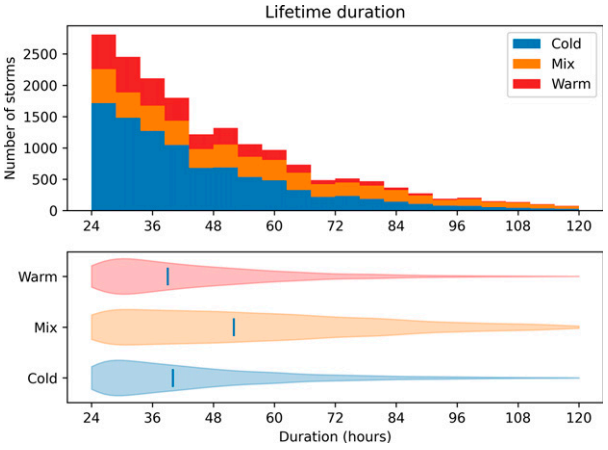

FIG. 2. Cyclone distribution based on system lifetime (all systems from 1950 to 2019). The violin plots use kernel density estimation to compute an empirical distribution of storm cases. The vertical blue lines in the violin plot denote the medians in the sample groups.

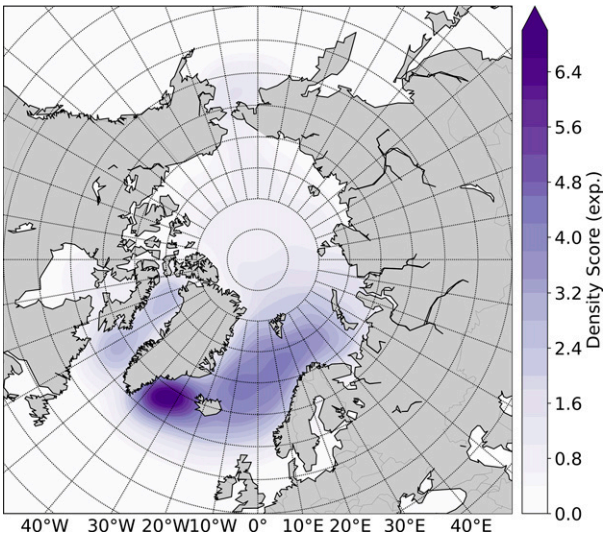

FIG. 3. Spatial distribution of the maritime cyclones detected in this study. The kernel density plot shows the probability score (exponential) of storm centers based on the haversine distance metric and a bandwidth of 0.04.

3. Results

a. *Validation*

It is critical to validate the efficacy of the tracking algorithm before addressing the tracking results for Arctic cyclones. First, we verified individual cyclone tracks to examine outliers. During the initial quality inspection of our tracking results, we discovered a small number of spurious systems that lasted for as long as 250 h, which likely resulted from the misrepresentation of multiple storm tracks into a single track. Because these life spans are highly unlikely, all tracks with a duration longer than 120 h were removed. These spurious tracks only constitute only about one percent of the total tracks and thus have limited impact on the climatology.

Track-to-track verifications were performed against Stoll et al.'s (2021) polar low dataset, which contains a total of 374 polar low tracks (a total of 263 systems and 404 tracks available in Stoll's supplemental material for the period 1999–2019). This climatology was also based on the hourly ERA5 reanalysis but was derived from an algorithm tracking 850-hPa vorticity maximum (Watanabe et al. 2016). The Stoll climatology was verified against AVHRR satellite images of polar lows compiled by Rojo et al. (2019). While the climatology excludes the synoptic scales, it does include cyclone tracks with an hourly time stamp and hence is somewhat comparable to the results obtained here.

Because the tracking algorithm developed herein included only the strong cyclones (vorticity greater than $0.5 \times 10^{-5}\ s^{-1}$) with life spans longer than 24 h, similar selection criteria were imposed on the Stoll list. Among 237 in the Stoll list that have a lifetime equal or longer than 12 h, our algorithm detected 180 matching tracks (75.9%), with each Stoll's track having more than 50% of the total storm centers accompanied by a nearby storm center within 150 km in our tracking results. When comparing the total number of cyclone centers instead of tracks, 7859 of 11 172 storm centers (70.3%) in the Stoll list have corresponding storm centers within a 150-km search radius in the tracking results presented here. In the next section, regional cyclone counts and seasonality are also compared with other climatologies wherein detailed track datasets are publicly unavailable (e.g., Smirnova et al. 2015; Stoll et al. 2018; Vessey et al. 2020).

An individual case is also examined in detail to demonstrate the efficacy of the tracking algorithm. The polar low of November 2013 in the Norwegian Sea was tracked by hand using Advanced Very High Resolution Radiometer (AVHRR) data (H. Situ 2020, personal communication; Fig. 1a) and was also captured in the Stoll list. The cyclone developed early on 18 November and tracked northward toward Bjørnøya (Bear Island), where it stalled and continued to intensify for over 30 h, and then propagated southeastward to the Barents Sea where it underwent cyclolysis. The tracking algorithm shows good agreement with manual tracking of the cyclone center, particularly once it was well developed, and during the complex period when the cyclone meandered around Bjørnøya. Figure 1b shows the 850-hPa relative vorticity from ERA5 over the life of the cyclone and demonstrates the complex transition between cold-core and warm-core (shaded) structures. During the first phase of intensification, the cyclone started to develop as a frontal cyclone (e.g., Fig. 1c; T1: 1300 UTC 18 November). As the cyclone meandered and continued to intensify, the circulation became more organized and retained this structure (Fig. 1c; T2: 0800 UTC 19 November) even as warm air started to converge into the cyclone core (Fig. 1b). When the cyclone finally began to propagate once more, it transitioned to an axisymmetric, warm-core system that, while rapidly weakening, demonstrated some convective mesocyclone characteristics (e.g., Fig. 1c; T3: 1200 UTC 20 November). The system later merged with a secondary depression apparent in Fig. 1c, during T3. This complex development is captured well by the ERA5 reanalysis, and both

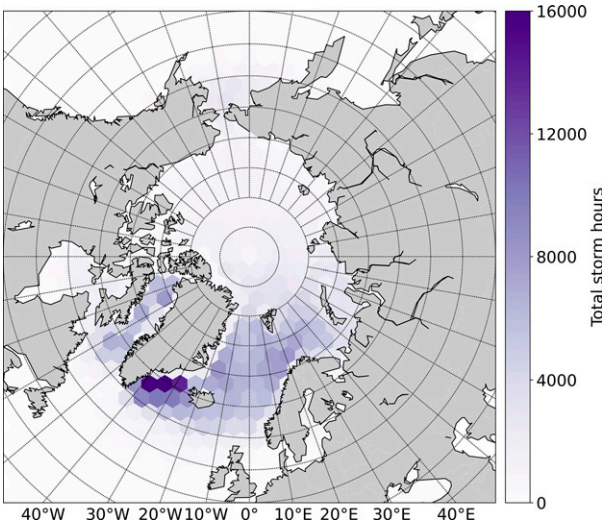

FIG. 4. Spatial distribution of Arctic cyclone hours detected in this study. The color of each hexagonal bin represents the total number of storm centers from 1950 to 2019 in the corresponding area.

the MSLP tracker and the vorticity tracker used by Stoll et al. (2021) closely aligned with the system track. The track developed here did provide a continuous result at around T2 whereas the vorticity tracker missed the system for around 15 h, thus causing a gap in the middle of the vorticity plot. More details about the MSLP tracking algorithm and its application for tropical cyclones can be found in Murakami et al. (2015) and Harris et al. (2016) for the efficacy of this approach.

b. *Spatial and temporal distributions*

It was determined that the use of relatively inclusive tracking criteria, which would yield all significant Arctic cyclones resolved by the ERA5 reanalysis, would be useful in developing an initial comprehensive climatology. Hence, the selection criteria used here avoid distinctions that may arise due to differing definitions of cyclone scales (polar lows in particular), by tracking every Arctic depression that meets a minimum threshold of intensity (maximum 10-m wind speed exceeding 15 m s^{-1} and minimum vorticity of 0.5×10^{-5} s^{-1} over a system's lifetime) and duration (greater than 24 h; see methods section). From this superset, it will be possible to select for cyclone characteristics as appropriate for different applications. This study has found a comparable frequency of cyclone cases to earlier climatologies, considering the spatial resolution and temporal coverage of the ERA5 product relative to the previous studies. For example, Smirnova et al. (2015) identified 637 polar low cases for the period 1995–2009 over the Norwegian and Barents Seas based on Special Sensor Microwave Imager (SSM/I) data, an average of 45.5 per season (from September to April). Stoll et al. (2018) detected 709 cases in total (50.6 per season) for the same period and approximately in the same area, using the ERA-Interim reanalysis. Within the similar geographical domain (20°W–60°E, 60°–80°N) as Smirnova et al. (2015), our algorithm detected a total of 1230 tracks (87.9 per season) for the same period. Using a more limited seasonal demarcation and counting only synoptic-scale cyclones north of 65°N, Vessey et al. (2020) used a vorticity criterion to detect around 116 cyclones per season in December–February (DJF) and 97 per season in June–August (JJA) for the period 1980–2017. In comparison, we identified 2818 cases (76 per season) in DJF and 806 cases (21 per season) in JJA between 1980 and 2017 over the same area. The difference in the track number is expected because Vessey et al. (2020) extensively tracked all the Arctic cyclones, including those with a terrestrial origin, whereas our study only focused on the maritime mesoscale systems.

Applying these criteria to the area north of 60°N, our tracking algorithm detected 10 555 maritime cyclones between 1979 and 2019 and 6896 between 1950 and 1978, representing a total of over 1 million storm hours. On average, 239.6 ± 14.3 cyclones are detected every year Arctic-wide during 1950–78 and 266.0 ± 20.5 for 1979–2019. In terms of average lifetime, the

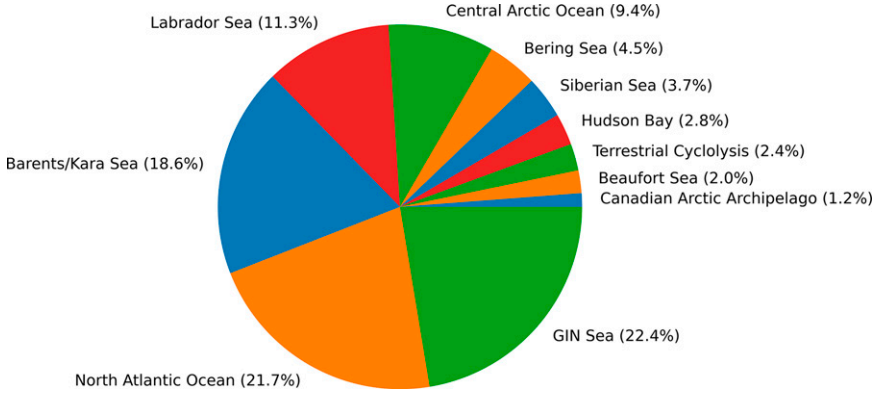

FIG. 5. Comparison of total storm hours at different Arctic sea sections from 1950 to 2019. The percentages in the pie chart represent fractions of the storm hours at a particular location to the total storm hours at all sections. The map annotation for each sea section can be found in Fig. 6, below.

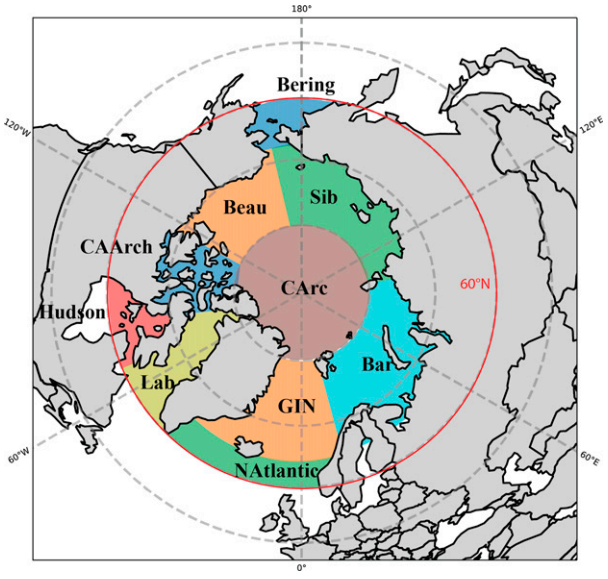

FIG. 6. Annotation for the Arctic sea sections used in Fig. 5. Note that a section of the Bering Sea falls out of the 60°N boundary.

systems during 1950–78 exhibited a mean duration of 47.1 ± 20.3 h, whereas those from 1979 to 2019 were not significantly different and with the same high variability, at 48.4 ± 21.1 hours. Figure 2 also distinguishes between cyclones that have cold cores throughout their entire life cycle—by far the majority—from cyclones that exhibit warm cores, and those that transition from one structure to the other. This latter, mixed, category, requires more systematic detection choices, as described in the methods section, to ensure that weak developments hovering in a barotropic environment do not artificially inflate this category. Cold-core systems are the most common type, with 9449 storms representing 54.1% of the total cases in the dataset. These cyclones tend to have a short median life span (40 h). Similarly, the warm-core systems (18.7%) tend to be short lived, with a median duration of 39 h. In contrast, cyclones that exhibit a combination of cold- and warm-core signals over their lifetimes—accounting for 27.2% (4745 tracks)—are more likely to be long-lived, with a median life span of 52 h. The warm and mix-core systems also exhibit higher intensity than the more common cold-core systems, with a median maximum 850 hPa vorticity of 4.80×10^{-5} s^{-1} as compared with 4.00×10^{-5} s^{-1} for cold-core systems. The considerable number of intense, long-lasting systems that transition (most typically from cold core to warm core) suggests that cyclogenetic forcing changes over the life cycles of many of these cyclones is a significant driver in the most impactful cases. These cyclones, such as the case of November 2013 described above, are the subject of ongoing, more detailed, structural analysis.

As noted earlier and in the methods, storms that originate over land are explicitly excluded from this analysis. The spatial distribution of all maritime cyclones north of 60°N for the period 1950–2019 is shown in Fig. 3 as kernel density estimation, and a corresponding hexagonal-bin plot that represents the storm hours is shown in Fig. 4. The distribution is consistent with earlier studies using different methods and data sources and indicates broad agreement in the centers of action for cyclones in the Arctic (Serreze 1995; Zahn and Von Storch 2008; Stoll et al. 2018; Vessey et al. 2020). In the North Atlantic Ocean, most Arctic cyclone activity is concentrated in the Denmark Strait between the southern tip of Greenland and western Iceland. The Norwegian Sea is a secondary center of action in the Atlantic sector. Indeed, it was in this region that polar lows were first characterized (Rasmussen and Turner 2003). The Barents and Kara Seas make up 18.6% of detected cyclone hours for the entire period, as compared with 22.4% in the Greenland–Iceland–Norwegian (GIN) Seas and 21.7% in the high North Atlantic (Figs. 5, 6). In the North Pacific, cyclones are typically less frequent; the algorithm detects cyclonic activity in the Bering Sea, making up just under 4.5% of cyclone hours. However, note that a large section of the Bering Sea was excluded from the tracking result because of the study

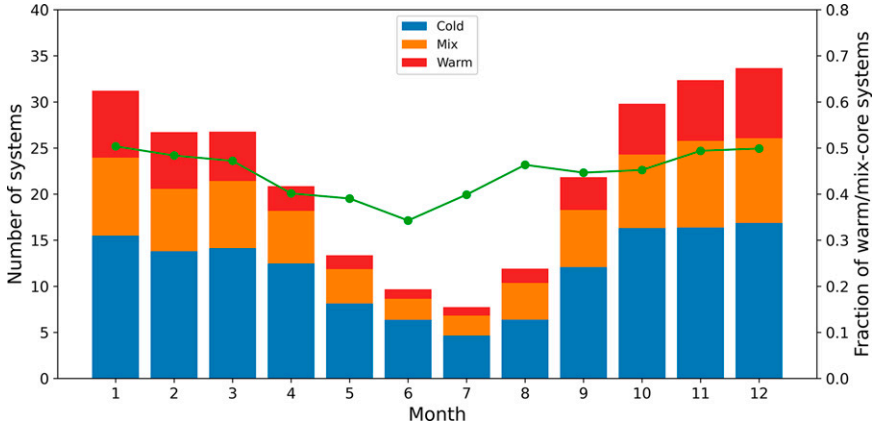

FIG. 7. Seasonal variation of the maritime cyclones detected in this study showing the monthly average number of cyclone tracks from 1950 to 2019 (bar chart; left *y* axis). The green line shows the ratio of warm- and mix-core cases to all systems (right *y* axis).

TABLE 2. Changes in Arctic cyclones characteristics from 1950 to 2019. The winter cases (DJF) are, when measured by minimum MSLP and maximum wind speed, more intense than those in other seasons. The summer cases (JJA) are the weakest but longest lasting ones. Here, MAM is March–May and SON is September–November. In each table cell, the left number is derived from the period of 1950–78 and the right number is derived from the period of 1979–2019.

Season	DJF	MAM	JJA	SON
Tracks per year	81.7; 92.6	54.4; 61.5	29.4; 27.5	77.7; 82.0
Duration (mean; h)	43.1; 44.3	46.3; 47.9	51.8; 52.5	46.9; 48.4
Duration (std dev; h)	18.7; 19.8	20.8; 21.5	23.5; 23.7	20.5; 21.7
Max 850-hPa vorticity (mean; s^{-1})	5.00×10^{-5}; 5.13×10^{-5}	4.38×10^{-5}; 4.54×10^{-5}	4.00×10^{-5}; 3.97×10^{-5}	4.56×10^{-5}; 4.60×10^{-5}
Max 850-hPa vorticity (std dev; s^{-1})	2.09×10^{-5}; 2.20×10^{-5}	1.71×10^{-5}; 1.80×10^{-5}	1.16×10^{-5}; 1.18×10^{-5}	1.81×10^{-5}; 1.76×10^{-5}
Min sea level pressure (mean; hPa)	978.69; 977.23	985.80; 984.90	988.33; 987.80	981.92; 982.30
Min sea level pressure (std dev; hPa)	14.97; 15.50	12.58; 13.23	8.22; 8.16	12.18; 12.31
Max wind speed (mean; m s^{-1})	19.97; 19.98	19.10; 19.13	17.35; 17.28	18.88; 18.78
Max wind speed (std dev; m s^{-1})	3.98; 4.01	3.43; 3.54	2.05; 2.33	3.29; 3.21

boundary of 60°N (Fig. 6). Some polar lows do occur in the sub-Arctic Bering Sea, but they are not subject to the analysis in this study. In the Beaufort and Siberian Seas, marine cyclogenesis is also rather rare (5.7%) although intense cyclones originating over the Siberian landmass have been observed (Lynch et al. 2003). As with earlier climatologies, polar lows and other Arctic cyclones are relatively rare poleward of the marginal ice zone—with around 9.4% of storm hours detected in the central Arctic Ocean—where baroclinicity is typically lower. A few of the cyclones detected by our algorithm that originate over the ocean go on to decay over land—these cyclones are indicated as "terrestrial cyclolysis" in Fig. 5 and represent only 2.4% of storm hours detected. As for earlier studies that addressed mesocyclones over limited areas and time periods, and those that addressed synoptic cyclones over the entire Arctic, the frequency of Arctic cyclones in this analysis follows a strong seasonal pattern. Stoll et al. (2018) noted that the "polar low season" in the Northern Hemisphere starts in October and ends in April. July–August typically generate a negligible number of polar low cases. Vessey et al. (2020) find a similar seasonal distribution for Arctic synoptic cyclones. This finding has been consistent over time: Zhang et al. (2004) and Sorteberg and Walsh (2008) used the National Centers for Environmental Prediction–National Center for Atmospheric Research reanalysis to detect synoptic-scale cyclones that demonstrated this seasonality. More focused regional climatologies based on radar and satellite observations, such as those of Noer et al. (2011) and Smirnova et al. (2015), found a similar winter peak in polar low frequency in the Nordic seas. In our study, cyclones detected in the ERA5 reanalysis demonstrate a similar seasonality (Fig. 7; Table 2): the highest frequency of Arctic maritime cyclones extends from October to April, and the highest number of cyclone tracks occur in November–January. Because of the relatively inclusive criteria adopted in this study with regard to the system strength and longevity, a considerable number of summer cases are detected. Summer systems (JJA) are longer-lived but considerably weaker than winter systems (DJF).

Figure 7 shows the seasonality associated with cyclones that have cold, warm, and mixed cores. From the beginning of the typical Arctic cyclone season until its peak in January, the ratio of warm-core and mixed cases (those that undergo a defined transition) to cold-core cases increases from about 0.45 to 0.50. The increased frequency of time periods in any cyclone's life cycle of warm-core characteristics during the winter is consistent with the increased surface fluxes of heat and moisture in the marginal ice zone due to relatively warm open water overlain by cold, dry air. Indeed, there is a significant proportion of systems in the peak months that are purely warm-core developments, which is rarely observed in the summer months. The fraction of warm-core and mixed type cyclones decreases dramatically in March to a minimum of around 0.35 in August.

Previous studies that have focused on polar lows more specifically have demonstrated insignificant change in cyclone frequency (by number of storms) over the past several decades (e.g., Stoll et al. 2018). In terms of synoptic storms in the Arctic, Vessey et al. (2020) also found no trend in their

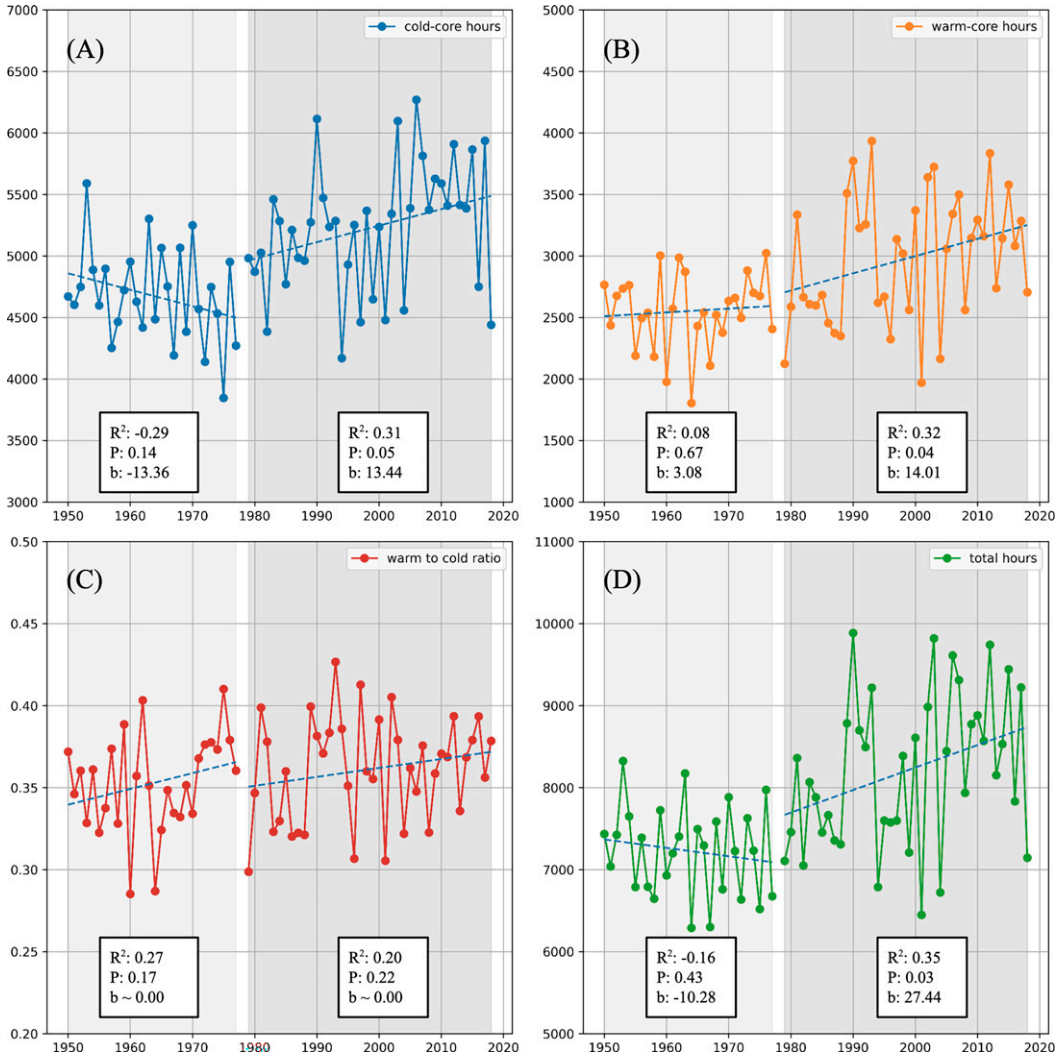

FIG. 8. Increasing storm hours during extended winter (October–March) over the extended Arctic region (north of 60°N) from 1950 to 2019: (a) Annual total cold-core hours (with negative warm-core signal); (b) annual total warm-core hours (with positive warm-core signal); (c) ratio of annual total cold-core to warm-core hours (no significant trend); (d) total cyclone hours detected.

frequency between 1980 and 2017. However, our analysis suggests that there is indeed a significant increase in cold-core, warm-core, and total cyclonic activity during the extended winter season (October–March) from 1979 to 2019 across the Arctic and sub-Arctic regions (Fig. 8). The ratio of warm-core to cold-core storm hours, however, indicates no significant change with a p value larger than 15%. In addition to an overall increase of storm hours, the seasonal variation of the storm activity also appears to be intensified when comparing the period of 1950–78 with 1979–2019 (Fig. 9). The latter period has a higher wintertime maximum (DJF) of total storm hours but a lower summertime minimum (JJA) than 1950–78.

The regional contribution for the increasing storm trend between 1979 and 2019 is shown in Fig. 10. Despite the large interannual variation, it is likely that these trends are driven in part by the changes in the high-latitude North Atlantic Ocean, the GIN Seas, and the Bering Sea. The physical mechanism driving the changes in frequency, however, requires further investigation.

4. Summary and discussion

This study demonstrates that the cyclone-tracking algorithm developed by Murakami et al. (2015) and Harris et al. (2016) successfully tracks Arctic meso-α- and synoptic-scale cyclones using the ERA5 reanalysis. The tracking accuracy is validated through intercomparisons of individual storm tracks, one example of which is shown here, along with comparisons with previous climatologies. Assuming a set of relatively inclusive tracking criteria and making use of the improvements in spatial and temporal resolution afforded by the ERA5 reanalysis, the algorithm's tracking results are

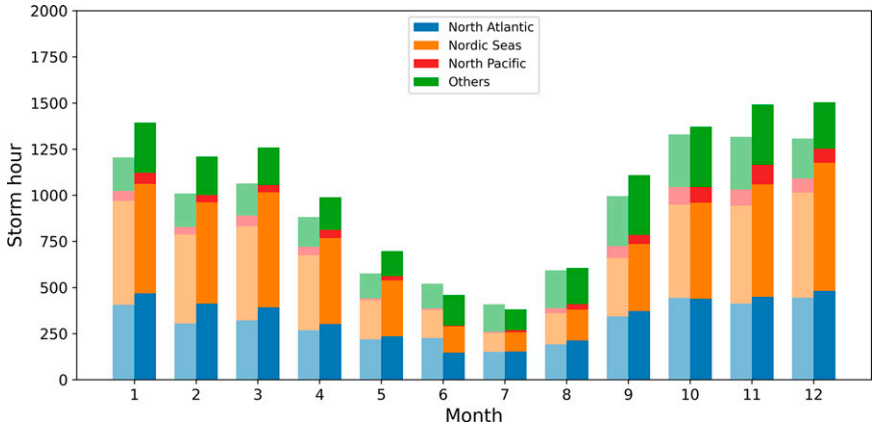

FIG. 9. Comparison of the storm seasonality between the period of 1950–78 (left bar of each pair) and 1979–2019 (right bar).

consistent with earlier studies in distribution and frequency. This study also develops a classification method that utilizes the 700-hPa temperature field and a search that accounts for vertical tilt to identify cold-core and warm-core cyclones, and cyclones that undergo transition from one type to the other (typically though not exclusively from cold to warm).This classification method will be used in future studies to assess forcing mechanisms throughout the cyclone life cycle.

The release of the 1950–2019 ERA5 reanalysis allows a better assessment of the significance of variations in storm frequency, intensity, and spatial distribution. The tracking scheme shows that cold-core systems make up half of the detected Arctic cyclones over the period 1950–2019. Most of the remaining systems experience transitions between a cold-core and a warm-core structure; these are most similar to the hybrid systems described in studies such as Lynch et al. (2003) and Terpstra et al. (2016). A significant increase was found in the long-term frequency of all cyclones as measured by total storm hours from 1979 to 2019, although the interannual variability is sufficiently large that it is difficult to disaggregate this finding to yield regional signals. The increase of total storm activities over the recent decades is noteworthy when compared with the trend from 1950 to 1978. There is some indication that the proportion of warm-core systems is rising, but there is no significant trend for mixed or hybrid systems. The spatial distribution and intensity of these maritime systems remains substantially the same. However, readers need to take caution when comparing the trends of storm activity,

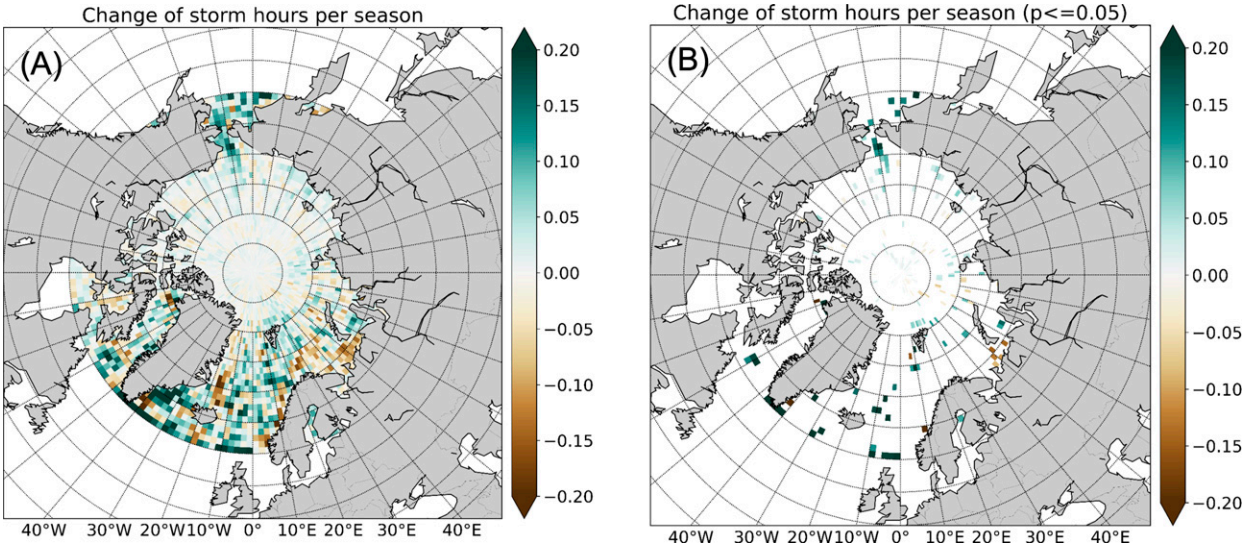

FIG. 10. Regional distribution of the increasing storm activity during extended winter season (October–March) from 1979 to 2019: (a) the change of storm hours per season (slope) is shown for each 2° (longitude) × 1° (latitude) grid box, and (b) as in (a), but only for the grid boxes with a p value of ≤0.05.

especially for the 1950–78 period because the extended ERA5 reanalysis was a preliminary release and has a different level of satellite data assimilation.

Future work will include the continued development of the tracking algorithm for Arctic cyclones. First, the tunable parameters used in this study were derived empirically based on a series of sensitivity analyses that demonstrated a straightforward relationship between the inclusivity of the threshold and the number of cyclones detected. These analyses also showed that a large proportion of these cyclones were relatively shallow, but that detections were not sensitive to assumptions about vertical tilt. Because threshold setting is likely to be dependent on the intended purpose of any climatology product, detailed sensitivity tests to select for target system types (by scale or structure) will yield a better understanding of the constraints of the tracking algorithm. Second, more extensive validation of tracking accuracy will require a larger number of cases to be evaluated from across the scale spectrum. In future work, this evaluation will focus on comparing the algorithm tracking results with polar low and synoptic cyclones climatologies compiled using satellite imagery (e.g., Noer et al. 2011; Smirnova et al. 2015).

Acknowledgments. We are thankful for the observational insights about polar lows provided by Helen Situ. We are grateful to Drs. Hiroyuki Murakami and Lucas M. Harris from the Geophysical Fluid Dynamics Laboratory in the National Oceanic and Atmospheric Administration Office of Oceanic and Atmospheric Research for sharing their cyclone-tracking algorithm. This study was supported by the National Science Foundation (CNH-S 1824829). This research was conducted using the Oscar supercomputer at the Center for Computation and Visualization at Brown University. The authors declare no competing interests.

Data availability statement. ERA5 data used in this study were retrieved from the Copernicus Climate Change Service Climate Data Store (https://cds.climate.copernicus.eu/cdsapp#!/home; accessed 13 February 2020 and 20 February 2021). The cyclone dataset generated by this study is open for access through Zenodo (https://doi.org/10.5281/zenodo.4479845).

REFERENCES

Bell, B., and Coauthors, 2021: The ERA5 global reanalysis: Preliminary extension to 1950. *Quart. J. Roy. Meteor. Soc.*, **147**, 4186–4227, https://doi.org/10.1002/qj.4174.

Blechschmidt, A. M., 2008: A 2-year climatology of polar low events over the Nordic seas from satellite remote sensing. *Geophys. Res. Lett.*, **35**, 2003–2007, https://doi.org/10.1029/2008GL033706.

Bracegirdle, T. J., and S. L. Gray, 2008: An objective climatology of the dynamical forcing of polar lows in the Nordic seas. *Int. J. Climatol.*, **28**, 1903–1919, https://doi.org/10.1002/joc.1686.

——, and ——, 2009: The dynamics of a polar low assessed using potential vorticity inversion. *Quart. J. Roy. Meteor. Soc.*, **135**, 880–893, https://doi.org/10.1002/qj.411.

Bromwich, D. H., A. B. Wilson, L. S. Bai, G. W. K. Moore, and P. Bauer, 2016: A comparison of the regional Arctic system reanalysis and the global ERA-Interim reanalysis for the Arctic. *Quart. J. Roy. Meteor. Soc.*, **142**, 644–658, https://doi.org/10.1002/qj.2527.

Brümmer, B., G. Müller, and G. Noer, 2009: A polar low pair over the Norwegian Sea. *Mon. Wea. Rev.*, **137**, 2559–2575, https://doi.org/10.1175/2009MWR2864.1.

Claud, C., G. Heinemann, E. Raustein, and L. McMurdie, 2004: Polar low le Cygne: Satellite observations and numerical simulations. *Quart. J. Roy. Meteor. Soc.*, **130**, 1075–1102, https://doi.org/10.1256/qj.03.72.

Dee, D. P., and Coauthors, 2011: The ERA-Interim reanalysis: Configuration and performance of the data assimilation system. *Quart. J. Roy. Meteor. Soc.*, **137**, 553–597, https://doi.org/10.1002/qj.828.

Deveson, A. C. L., K. A. Browning, and T. D. Hewson, 2002: A classification of FASTEX cyclones using a height-attributable quasi-geostrophic vertical-motion diagnostic. *Quart. J. Roy. Meteor. Soc.*, **128**, 93–117, https://doi.org/10.1256/00359000260498806.

Douglas, M. W., M. A. Shapiro, L. S. Fedor, and L. Saukkonen, 1995: Research aircraft observations of a polar low at the east Greenland Ice edge. *Mon. Wea. Rev.*, **123**, 5–15, https://doi.org/10.1175/1520-0493(1995)123<0005:RAOOAP>2.0.CO;2.

Emanuel, K. A., and R. Rotunno, 1989: Polar lows as Arctic hurricanes. *Tellus*, **41A**, 1–17, https://doi.org/10.1111/j.1600-0870.1989.tb00362.x.

Føre, I., J. E. Kristjánsson, Ø. Saetra, Ø. Breivik, B. Røsting, and M. Shapiro, 2011: The full life cycle of a polar low over the Norwegian Sea observed by three research aircraft flights. *Quart. J. Roy. Meteor. Soc.*, **137**, 1659–1673, https://doi.org/10.1002/qj.825.

——, ——, E. W. Kolstad, T. J. Bracegirdle, Ø. Saetra, and B. Røsting, 2012: A "hurricane-like" polar low fuelled by sensible heat flux: High-resolution numerical simulations. *Quart. J. Roy. Meteor. Soc.*, **138**, 1308–1324, https://doi.org/10.1002/qj.1876.

Harris, L. M., S. J. Lin, and C. Y. Tu, 2016: High-resolution climate simulations using GFDL HiRAM with a stretched global grid. *J. Climate*, **29**, 4293–4314, https://doi.org/10.1175/JCLI-D-15-0389.1.

Haualand, K., and T. Spengler, 2020: Direct and indirect effects of surface fluxes on moist baroclinic development. *J. Atmos. Sci.*, **77**, 3211–3225, https://doi.org/10.1175/JAS-D-19-0328.1.

Hennermann, K., and P. Berrisford, 2018: What are the changes from ERA-Interim to ERA5 and ERA5-Land? ECMWF, https://confluence.ecmwf.int/pages/viewpage.action?pageId=74764925.

Hersbach, H., and Coauthors, 2020: The ERA5 global reanalysis. *Quart. J. Roy. Meteor. Soc.*, **146**, 1999–2049, https://doi.org/10.1002/qj.3803.

Hoffmann, L., and Coauthors, 2018: From ERA-Interim to ERA5: Considerable impact of ECMWF's next-generation reanalysis on Lagrangian transport simulations. *Atmos. Chem. Phys.*, **19**, 3097–3124, https://doi.org/10.5194/acp-19-3097-2019.

Joly, A., and Coauthors, 1997: The Fronts and Atlantic Storm-Track Experiment (FASTEX): Scientific objectives and experimental design. *Bull. Amer. Meteor. Soc.*, **78**, 1917–1940, https://doi.org/10.1175/1520-0477(1997)078<1917:TFAAST>2.0.CO;2.

Lynch, A. H., E. N. Cassano, J. J. Cassano, and L. R. Lestak, 2003: Case studies of high wind events in Barrow, Alaska:

Climatological context and development processes. *Mon. Wea. Rev.*, **131**, 719–732, https://doi.org/10.1175/1520-0493(2003)131<0719:CSOHWE>2.0.CO;2.

McInnes, H., J. Kristiansen, J. E. Kristjánsson, and H. Schyberg, 2011: The role of horizontal resolution for polar low simulations. *Quart. J. Roy. Meteor. Soc.*, **137**, 1674–1687, https://doi.org/10.1002/qj.849.

Michel, C., A. Terpstra, and T. Spengler, 2018: Polar mesoscale cyclone climatology for the Nordic seas based on ERA-Interim. *J. Climate*, **31**, 2511–2532, https://doi.org/10.1175/JCLI-D-16-0890.1.

Murakami, H., and Coauthors, 2015: Simulation and prediction of category 4 and 5 hurricanes in the high-resolution GFDL HiFLOR coupled climate model. *J. Climate*, **28**, 9058–9079, https://doi.org/10.1175/JCLI-D-15-0216.1.

Neu, U., and Coauthors, 2013: IMILAST: A community effort to intercompare extratropical cyclone detection and tracking algorithms. *Bull. Amer. Meteor. Soc.*, **94**, 529–547, https://doi.org/10.1175/BAMS-D-11-00154.1.

Noer, G., Ø. Saetra, T. Lien, and Y. Gusdal, 2011: A climatological study of polar lows in the Nordic seas. *Quart. J. Roy. Meteor. Soc.*, **137**, 1762–1772, https://doi.org/10.1002/qj.846.

Nordeng, T. E., and E. A. Rasmussen, 1992: A most beautiful polar low. A case study of a polar low development in the Bear Island region. *Tellus*, **44A**, 81–99, https://doi.org/10.3402/tellusa.v44i2.14947.

Parsons, D. B., and Coauthors, 2017: THORPEX research and the science of prediction. *Bull. Amer. Meteor. Soc.*, **98**, 807–830, https://doi.org/10.1175/BAMS-D-14-00025.1.

Petrov, A. N., and Coauthors, 2016: Arctic sustainability research: Toward a new agenda. *Polar Geogr.*, **39**, 165–178, https://doi.org/10.1080/1088937X.2016.1217095.

Rasmussen, E., 1979: The polar low as an extratropical CISK disturbance. *Quart. J. Roy. Meteor. Soc.*, **105**, 531–549, https://doi.org/10.1002/qj.49710544504.

——, and J. Turner, 2003: *Polar Lows: Mesoscale Weather Systems in the Polar Regions.* Cambridge University Press, 632 pp.

Rojo, M., C. Claud, G. Noer, and A. M. Carleton, 2019: In situ measurements of surface winds, waves, and sea state in polar lows over the North Atlantic. *J. Geophys. Res. Atmos.*, **124**, 700–718, https://doi.org/10.1029/2017JD028079.

Sardie, J. M., and T. T. Warner, 1983: On the mechanism for the development of polar lows. *J. Atmos. Sci.*, **40**, 869–881, https://doi.org/10.1175/1520-0469(1983)040<0869:OTMFTD>2.0.CO;2.

Serreze, M. C., 1995: Climatological aspects of cyclone development and decay in the Arctic. *Atmos.–Ocean*, **33**, 1–23, https://doi.org/10.1080/07055900.1995.9649522.

——, and A. P. Barrett, 2008: The summer cyclone maximum over the central Arctic Ocean. *J. Climate*, **21**, 1048–1065, https://doi.org/10.1175/2007JCLI1810.1.

——, A. H. Lynch, and M. P. Clark, 2001: The Arctic frontal zone as seen in the NCEP–NCAR reanalysis. *J. Climate*, **14**, 1550–1567, https://doi.org/10.1175/1520-0442(2001)014<1550:TAFZAS>2.0.CO;2.

Smirnova, J., and P. Golubkin, 2017: Comparing polar lows in atmospheric reanalyses: Arctic system reanalysis versus ERA-Interim. *Mon. Wea. Rev.*, **145**, 2375–2383, https://doi.org/10.1175/MWR-D-16-0333.1.

——, ——, L. P. Bobylev, E. V. Zabolotskikh, and B. Chapron, 2015: Polar low climatology over the Nordic and Barents seas based on satellite passive microwave data. *Geophys. Res. Lett.*, **42**, 5603–5609, https://doi.org/10.1002/2015GL063865.

Sorteberg, A., and J. E. Walsh, 2008: Seasonal cyclone variability at 70°N and its impact on moisture transport into the Arctic. *Tellus*, **60A**, 570–586, https://doi.org/10.1111/j.1600-0870.2008.00314.x.

Stoll, P. J., R. G. Graversen, G. Noer, and K. Hodges, 2018: An objective global climatology of polar lows based on reanalysis data. *Quart. J. Roy. Meteor. Soc.*, **144**, 2099–2117, https://doi.org/10.1002/qj.3309.

——, T. Spengler, A. Terpstra, and R. G. Graversen, 2021: Polar lows—Moist baroclinic cyclones in four different vertical wind shear environments. *Wea. Climate Dyn.*, **2**, 19–36, https://doi.org/10.5194/wcd-2-19-2021.

Terpstra, A., T. Spengler, and R. W. Moore, 2015: Idealised simulations of polar low development in an Arctic moist-baroclinic environment. *Quart. J. Roy. Meteor. Soc.*, **141**, 1987–1996, https://doi.org/10.1002/qj.2507.

——, C. Michel, and T. Spengler, 2016: Forward and reverse shear environments during polar low genesis over the northeast Atlantic. *Mon. Wea. Rev.*, **144**, 1341–1354, https://doi.org/10.1175/MWR-D-15-0314.1.

——, I. A. Renfrew, and D. E. Sergeev, 2021: Characteristics of cold air outbreak events and associated polar mesoscale cyclogenesis over the North Atlantic region. *J. Climate*, **34**, 4567–4584, https://doi.org/10.1175/JCLI-D-20-0595.1.

Vessey, A. F., K. I. Hodges, L. C. Shaffrey, and J. J. Day, 2020: An inter-comparison of Arctic synoptic scale storms between four global reanalysis datasets. *Climate Dyn.*, **54**, 2777–2795, https://doi.org/10.1007/s00382-020-05142-4.

Watanabe, S. I., H. Niino, and W. Yanase, 2016: Climatology of polar mesocyclones over the Sea of Japan using a new objective tracking method. *Mon. Wea. Rev.*, **144**, 2503–2515, https://doi.org/10.1175/MWR-D-15-0349.1.

Wernli, H., and C. Schwierz, 2006: Surface cyclones in the ERA-40 dataset (1958–2001). Part I: Novel identification method and global climatology. *J. Atmos. Sci.*, **63**, 2486–2507, https://doi.org/10.1175/JAS3766.1.

Yanase, W., and H. Niino, 2005: Effects of baroclinicity on the cloud pattern and structure of polar lows: A high-resolution numerical experiment. *Geophys. Res. Lett.*, **32**, L02806, https://doi.org/10.1029/2004GL020469.

——, ——, I. Watanabe Si, K. Hodges, M. Zahn, T. Spengler, and I. A. Gurvich, 2016: Climatology of polar lows over the Sea of Japan using the JRA-55 reanalysis. *J. Climate*, **29**, 419–437, https://doi.org/10.1175/JCLI-D-15-0291.1.

Zahn, M., and H. Von Storch, 2008: A long-term climatology of North Atlantic polar lows. *Geophys. Res. Lett.*, **35**, L22702, https://doi.org/10.1029/2008GL035769.

——, M. Akperov, A. Rinke, F. Feser, and I. I. Mokhov, 2018: Trends of cyclone characteristics in the Arctic and their patterns from different reanalysis data. *J. Geophys. Res. Atmos.*, **123**, 2737–2751, https://doi.org/10.1002/2017JD027439.

Zappa, G., L. Shaffrey, and K. Hodges, 2014: Can polar lows be objectively identified and tracked in the ECMWF operational analysis and the ERA-Interim reanalysis? *Mon. Wea. Rev.*, **142**, 2596–2608, https://doi.org/10.1175/MWR-D-14-00064.1.

Zhang, X., J. E. Walsh, J. Zhang, U. S. Bhatt, and M. Ikeda, 2004: Climatology and interannual variability of Arctic cyclone activity: 1948–2002. *J. Climate*, **17**, 2300–2317, https://doi.org/10.1175/1520-0442(2004)017<2300:CAIVOA>2.0.CO;2.